Rodríguez-Millán, M.; Tan, L. B.; Tse, K.M.; Lee, H.P.; Miguélez, M.H. Effect of full helmet systems on human head responses under blast loading. *Materials and Design* 117 (2017) 58–71.

DOI: 10.1016/j.matdes.2016.12.081

GOBIERNO DE ESPAÑA MINISTERIO DE ECONOMÍA, INDUSTRIA Y COMPETITIVIDAD

UNIÓN EUROPEA FONDO EUROPEO DE DESARROLLO REGIONAL "Una manera de hacer Europa"

UNIÓN EUROPEA FONDO EUROPEO DE DESARROLLO REGIONAL "Una manera de hacer Europa"

Project RTC-2015-3887-8

Effect of full helmet systems on human head responses under blast loading

M. Rodríguez-Millán [a,*], L.B Tan [b], K . M . T s e [b,c], H . P . L e e [b], M.H Miguélez [a]

[a] Department of Mechanical Engineering, University Carlos III of Madrid, Avda. de la Universidad 30, 28911 Leganés, Madrid, Spain
[b] Department of Mechanical Engineering, National University of Singapore, 9 Engineering Drive 1, 117576, Singapore
[c] Biomechanical Research Group, Department of Mechanical Engineering, University of Melbourne, Parkville, VIC 3010, Australia

HIGHLIGHTS

- The effects of complementary systems added to the basic helmet configuration were numerically analyzed for a given mass of TNT.
- The protective equipment reduced brain pressures by 5 times and protected the head from skull fractures.
- Serious injuries may occur for the helmet with only one of the individual protective equipment

Keywords:
Combat helmet design
Mandibular guard
Visor
Blast simulation
Head modeling
Traumatic brain injury (TBI)
Intracranial pressure (ICP)

GRAPHICAL ABSTRACT

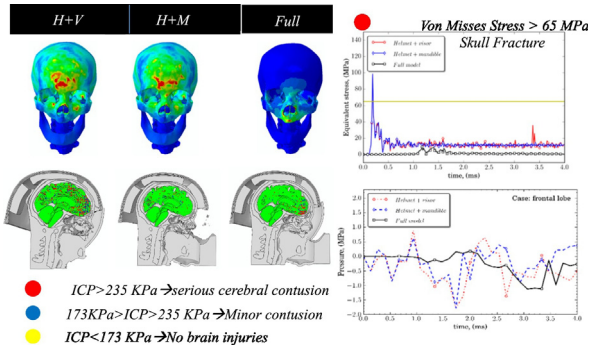

ABSTRACT

This paper focuses on helmet design for head protection under blast threats. It is presented a numerical investi-gation of the head response accruing to blast loads on helmet protective systems. Various combinations of the helmet, visor and mandible guard were numerically analyzed for a given mass of TNT at a distance to the target representing an anti-vehicle buried mine threat. Limited published articles on the subject are available in the sci-entific literature. In this paper, a 3D head–helmet numerical model for blast analyses is developed in the finite element code ABAQUS/Explicit. The results showed that individual protective systems are not effective enough to mitigate the damage caused by blast loading. The complete protective equipment reduces the pressures on the brain by up to 5 times and ensures that no fracture in the skull appears. This numerical study aims to provide helmet manufacturers and users with some insight in what possible brain injuries are to be expected in various blast scenarios so as to help in better diagnosis of unsuspected brain injury.

1. Introduction

Traumatic Brain Injury (TBI) has become an important societal problem because of the common occurrence of this type of lesion. In both civilian and military populations, most injuries (around 76%–83%) can be classified as mild TBI (mTBI) [1,2]. Although motor-vehicle, sport and work-related accidents are also examples of TBI in the civil society, TBI are commonly more severe and sometimes deadly in the armed conflicts and the terrorist activities due to intensive use improvised explosive devices (IED) as weapons that has led to the prevalence of blast-induced traumatic brain injury (bTBI) [3].

* Corresponding author.
E-mail address: mrmillan@ing.uc3m.es (M. Rodríguez-Millán).

The blast-induced traumatic brain injury (bTBI) has been found to be >60% of the TBI cases caused by blast explosions in conflicts such as Iraq and Afghanistan [4]. The analysis of the impact of military conflicts on TBI has been widely analyzed in the literature, see for instance [5,6].

Previous work in the literature has shown consensus concerning a conceptual classification of blast-related brain injury mechanisms [7,8]. It is assumed that blast injuries can be categorized in terms of damage mechanisms into primary, secondary, tertiary, and quaternary injuries. The primary blast induced damage mechanism refers to the overpressurization shock wave associated with high-energy explosives. Secondary injuries are due to the action of flying debris thrown by the blast. Tertiary blast injuries result from the victim being thrown into stationary objects by the blast. Finally, quaternary injuries are caused by electromagnetic pulses, heat, or toxic products generated by the blast. In common military situations, soldiers may be exposed to injuries caused by any of these different mechanisms. However, primary and secondary injuries are found to be more harmful for soldiers [9]. The understanding of brain injury mechanisms is a great challenge in research due to the difficulty of performing in vivo experimental testing. As it was explained before, different mechanical events can result in brain and skull injuries in the human head. The damage variables and their critical values indicative of tissue mechanical damage should be established.

Intracranial pressure (ICP), principal strains and shear strains with the pulse duration are the most commonly used injury metrics, given that an increased, or decreased pressure, strains lead to damaged neurons and blood vessels, torn of brain tissues, thus to brain damage, and therefore strong metrics for brain injuries [10–12]. Intracranial pressure (ICP) is usually used as a brain injury metric in the literature. ICP is defined as the pressure exerted by the cranium on the brain tissues and cerebrospinal fluid (CSF). Several authors have proposed different injury thresholds [12–14]. Ward et al. [13] used numerical models to predict intracranial pressure. The author concluded that a peak pressure of >235 kPa could result in serious brain injury; however, no brain injury occurs when the ICP < 173 kPa and moderate to severe injury appears when 173 kPa < ICP < 235 kPa. Zhang et al. [12] proposed 90 ± 24 kPa for TBI onset based on data from sports collisions, while Kleiven [14] proposed 66 kPa for a 50% probability of concussion. Researchers dealing with numerical head blast simulations have implemented these damage criterions for brain injury assessment [15–17]. The overall head kinematics in terms of head acceleration are an alternative method for evaluating brain injury in the automotive industry. The most widely used of such criteria is the Head Injury Criterion (HIC) which is based on the probability of injury due to global motion of the head; however, the intracranial mechanical response (local effects) is not taken into account.

Although severe brain injury may occur in absence of skull fracture, this mechanism is one of the most frequent occurring types of head injuries. The stress thresholds in the cranial bone were already reported in early works developed in the 70s, such as [18–19]. The fracture stress were reported to range between 48–128 MPa for cortical bone and between 32–74 MPa for trabecular bone. For instance, Wood [18] established the tensile fracture stress for skull around 65 MPa.

In this work, intracranial pressure (ICP), principal strains, shear strains and skull stress have been used in the assessment for brain injuries and skull fractures, respectively.

Full protection against the most common blast damage mechanism (primary and secondary injuries) requires the use of proper personal equipment. Combat helmets are considered the main head protection equipment for the soldiers. The Advanced Combat Helmet (ACH) head protection system equipped with polyurea suspension pads is commonly used by military forces. Most works in the literature have been focused on evaluating ballistic impact response of combat helmets; however, currently, >50% of the TBI cases are caused by blast explosions [20]. Helmet systems can reduce the biomechanical effects of blast on a human head, however the influence of combat helmets configuration on the blast-induced mechanical loads in the brain, has not been thoroughly analyzed.

Experimental tests in blast induced injuries have been limited, for moral considerations and set-up complexity, to animal tests, mainly on pig or rat [21,22] and on (simplified) surrogate human head models [23,24]. The results of both methods may be used to extrapolate the injury thresholds for the human head.

Despite the importance of carrying out experimental tests and because of their complex implementation, numerical modeling provides an invaluable tool for characterizing the physics of the problem in terms of relevant mechanical variables such as stress, strain, and acceleration. Different numerical models of human head and combat helmet have been developed and applied to study brain injury induced by impact loadings, see for instance recent contributions in [25–27]. Recently, numerical investigations related to explosive blast, human head and combat helmet design have also been developed, main contributions are summarized in the following.

Taylor and Ford [28] and Taylor et al. [29] established the role of stress wave interactions in the onset of traumatic brain injury (TBI) from exposure to explosive blast. It is worth noting that the studies did not take into account the use of personal protection. Elevated pressure, volumetric tension, and deviatoric stress in focal areas of the brain were revealed.

Moore et al. [30] used a numerical model of the head to analyze two cases of explosion (5.2 atmospheric pressure blast and 18.6 atmospheric pressure blast), and impact on a head (5 m/s). The highest level of pressure and stress were located at the right temporal region, since it was the incidence zone for the explosion. The study did not take into account the personal protection.

Grujicic et al. [31] developed a CAD head model including brain, CSF, small brain, brainstem, pituitary gland, and skull. The head was protected by a helmet system (combat helmet + polyuria). They investigated the potential of polyurea (a segmented, thermo-plastically cross-linked elastomer) as a blast-impact mitigating helmet suspension-pad material and compared it with the performance of conventional Ethylene-Vinyl-Acetate (EVA) foam. They concluded that polyurea is a preferred choice in helmet suspension-pad applications.

Zhang et al. [32] used a numerical simple head and combat helmet model to analyze the head orientation-dependent responses. Results obtained with the model suggested that directional-specific tolerance criteria are needed for the helmet design in order to offer omni-directional protection for the human head.

Tan et al. [14] employed a FE head model and PASGT (Personnel Armour System Ground Troops) helmet model developed by Lee and Gong [33] to analyze the influence of the combat helmet under blast loading. This study recommended better protection at the sides and rear of the helmet through the use of foam pads in order to reduce wave entry into the helmet. The consecutive frontal blasts scenario resulted in higher ICPs compared with impact from a single frontal blast.

Singh et al. [17] compared two detailed finite element (FE) head models applied to three blast load cases, in terms of brain tissue response and head kinematics. In general, both the sagittal and transverse models predicted lower principal strains than those seen in automotive crash scenarios. However, the model did not take into account personal protections in the head.

Jenson and Unnikrishnan [34] simulated the blast loadings on a simple FE head model with the use of nanocomposite materials in the helmet. A comparison between CNT enhanced helmet and the original advanced combat helmet (ACH) was made and showed the efficacy of both types of helmets in the protection of the brain. The major disadvantage of this work is that the skull and helmet models were too simplified and showed limitations.

These studies revealed the need for enhancing the virtual head models. The FE human head founded in the literature reproduce quite well the effects in the head during the blast although they may be considered simplified. In our work, we use a sophisticated FE human head

with detailed anatomical features in comparison with some founded in the literature. We have considered in our model: skull, nasal cartilages, soft tissue, white matter, grey matter, the cerebral peduncle for the intracranial contents; and for the ventricular system, bilateral lateral ventricles, third and fourth ventricle. In addition, in the literature, they have analyzed the blast mitigation effectiveness of only the basic helmet based on the ACH. To the authors' best knowledge, few investigations have focused on influence of complete helmet systems (including mandible guard and visor) in order to minimize the effect of blast loadings. The effect of these complementary systems is highlighted in the work developed by Mott et al. [35], who revealed that the use of face shield can reduce the peak pressure on the forehead and the eyes by a factor of roughly 3 and 5, respectively.

This work focuses on the effect of complementary systems added to the basic helmet configuration. A design of visor and mandible guard, which are similar to those in the Helmet Electronics and Display system — Upgradeable Protection (HEaDS-UP) program, is included due to the need in improving eye and face protection; in addition to its effect on head injuries due to blast. These protective equipments' performance is evaluated through numerical simulations in combination with the use of the ACH under blast loading. A numerical model based on finite elements was developed simulating the biomechanical response of the human head and the mechanical behavior of the protections allowing the study of the interaction between blast loading and head. Various combinations of helmet, visor and mandible guard were simulated in order to determine the best configuration. The results provide insights on the blast mitigation characteristics of the existing helmet, as well as suggest a possible strategy to further mitigate blast effects on the brain using helmet systems.

2. Methods and materials

2.1. Model description

The procedure for the model creation of the three-dimensional models of human head and helmet requires the use of different software packages. The steps between the image capture of the complex head/helmet system and the numerical analysis of its behavior under blast actions is illustrated in Fig. 1.

Geometrical information of both the human skull and brain are obtained from axial computed tomography (CT) and magnetic resonance imaging (MRI) images while the geometry of an advanced combat helmet (ACH) is extracted using a Siemens Sonotron Sensation CT scanner. These medical images were then imported into Mimics v13.0-v14.0 (Materialise, Leuven, Belgium) for segmentation, before the models were discretized using a semi-automatic technique in HyperMesh v10.0 (Altair HyperWorks, Troy, MI, USA). The detailed information of the development and validation of the FE human head and combat helmet models can be found in Tse and co-authors [36,37]. The blast analyses are performed using a commercial FE code, ABAQUS Explicit (Dassault Systemes SIMULIA, RI, USA), in order to analyze the influence of the helmet and its complementary systems. The helmet has been designed to closely resemble the American Combat Helmet prototype of the program called Helmet Electronics and Display system — Upgradeable Protection (HEaDS-UP) due to need improve eye and face protection. Both provide fragmentation protection for the face. The main attractive of our design or the HEaDS-UP prototype is that the set-up is a modular system. Detailed models of the ACH, conceptual visor and mandible guard, and head model are shown in Fig. 2.

2.1.1. Helmet model

The full helmet model consists of the ACH, 7-padding interior foams, visor and mandible guard. The number of elements, element types and average size are provided in Table 1. The behavior of helmet and the inner foams was validated against ballistic experiments in terms of maximum deflection of the helmet, the depth and diameter of impression, the projectile's rebound velocity and observed failure modes. More details of the validation can be found in a previous work of the authors [37].

2.1.2. Human head model

The FE model of human head includes the skull, nasal cartilages, soft tissue, white matter, grey matter, the cerebral peduncle for the intracranial; and for the ventricular system, bilateral lateral ventricles, third and fourth ventricle was developed, as shown in Fig. 3. The model weighs 4.73 kg and consists of 1,337,903 linear tetrahedral elements with the average element size of 1.57 mm and aspect ratio of 1.61.

The cerebrospinal fluid (CSF) between the skull and the brain tissue was modeled using three layers of solid elements according to several authors [38,39], the mechanical properties of these elements represents fluid behavior. The head model has been validated against the experimental tests from Nahum et al. [40], Trosseille et al. [41] and Hardy et al. [42] in terms of the intracranial pressure (ICP) and the relative intracranial motion data of the three cadaveric tests. More details of the development and validation of the FE head model are provided in our previous study [36]. In this previous work, the accuracy of the head model was demonstrated by comparison with three cadaveric experimental data at various anatomical landmarks. Despite the interest of developing a convergence study in order to state the optimum element size of all model components, this approach was not taken due to the complexity of the mesh. It is worth noting that mesh convergence analysis for head model is rarely developed for such biological analysis because the head model requires segmentation and remeshing leading to extremely elevated computational cost. Instead of convergence analysis the validation with three cadaveric experiments was carried out, proving that the FE model is adequate in predicting biomechanical parameters in both dynamic/ballistic impacts [36,37].

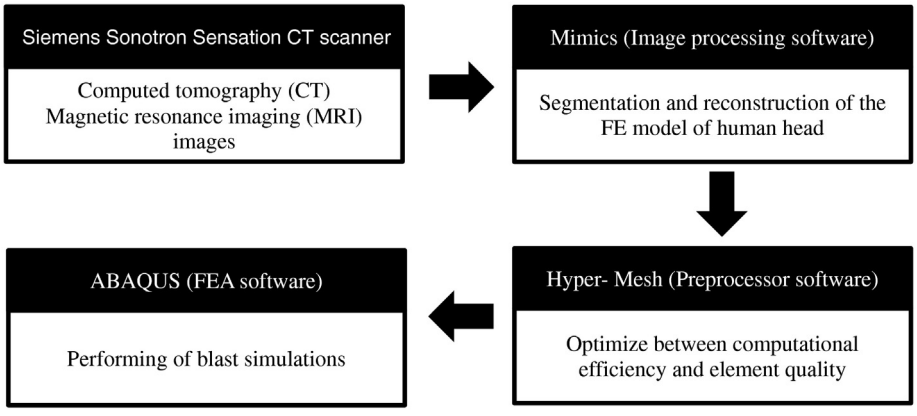

Fig. 1. Methodology for the development of the numerical model.

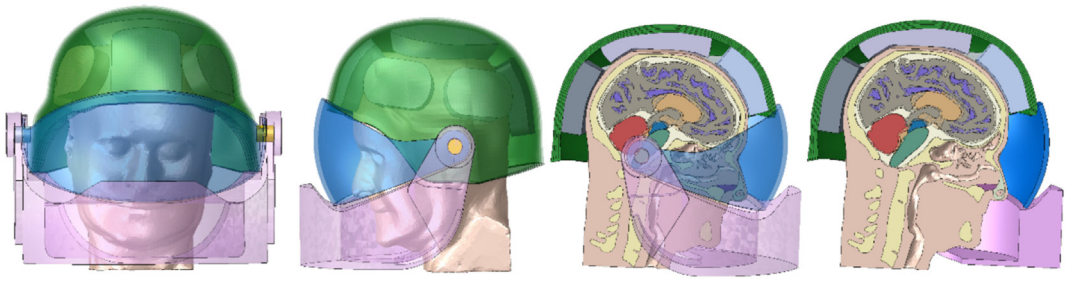

Fig. 2. Scheme of the numerical model developed in this work.

2.2. Material properties

2.2.1. Helmet modeling

The main component of the personal protection is the Advanced Combat Helmet (ACH), which is made of Kevlar composite. The behavior of the Kevlar composite was modeled through the introduction of a user subroutine VUMAT assuming elastic behavior up to failure.

Failure was predicted using the Hashin fabric failure criteria [43] implemented in a VUMAT user subroutine, modified by Tan et al. [15] -see Table 2-. Numerous studies on low and high-velocity impact have demonstrated the accuracy of Hashin failure criteria to model the dynamic behavior of woven composites, see for example [27,44,45].

The parameters in Table 2 are the following: σ_{11}, σ_{22}, and σ_{33}, are the stresses in longitudinal, transverse and through-thickness direction respectively; σ_{12}, σ_{23}, and σ_{13}, are the shear stresses; X_{1T} and X_{2T} are the tensile strengths in warp and weft directions; $S_{12,}$ $S_{13,}$ and $S_{23,}$ are the transverse shear strengths. Failure occurs when any damage variable (d_{ij}) reaches the value 1.

The reduction of elastic properties could lead to distorted elements involving numerical problems, thus the model requires the use of an element erosion criterion. The stresses on a damaged element drop to values close to zero while large deformations appear. These elements do not contribute to the strength or the stiffness of the plate, but they can cause lack of convergence during simulation and instability problems. The erosion criterion based on maximum strain criteria, was implemented in the VUMAT subroutine to remove the distorted elements. After each time increment the longitudinal strains (ε_{11}, ε_{22} and ε_{33}) were evaluated, and the element was removed if one of the strains reached a critical value. The strains used in the erosion criterion were $\varepsilon_{11}^{max} = 1$, $\varepsilon_{22}^{max} = 1$ and $\varepsilon_{33}{}^{max} = 1$, high enough to prevent the deletion of elements that contribute to the stiffness and strength of the target. Thus, numerical problems were avoided and at the same time only strongly damaged elements were deleted retaining resistant elements. Since element deletion is controlled by the VUMAT user subroutine, distortion control was not used. Thus, the objective of the erosion criterion is to avoid convergence problems due to the distortion of elements previously degraded. This approach is neither numerically inaccurate nor unsupported because for Kevlar yarns, their typical fiber failure strains are usually <10%. Thus, having the element erosion criteria set at 100% of strain (or double its original length) is conservative enough. The damage and degradation model as described in the main text degrades both the strengths and stiffnesses of the Kevlar composite over time. However, as the software do not actively remove elements which hold no load or stiffness (due to material failure), a criteria has to be set to perform this operation. These elements without any stiffness will deform or elongate enormously which can cause convergence issues, thus elements are removed as it is commonly done for this kind of dynamic analyses. In the case of blast, erosion only affects very few elements with negligible effect in the global response of the head/helmet model.

The parameters for Hashin model were already used by the authors in [15,27] and obtained from Gong et al. [46], Table 3.

2.2.2. Helmet complementary systems modeling

The protection of the helmet is enhanced when it is combined with complementary systems, mainly inner foam, mandible guard and visor. The behavior of these components is described in this section.

- *Interior foams*

The interior foams were modeled using the Low Density Foam material model available in ABAQUS which is intended for low-density, highly compressible elastomeric foams with significant rate sensitive behavior, such as polyurethane foam. The model uses a pseudo visco-

Table 1
Number of elements of combat helmet.

Components	N°. elements	Type	Average size
ACH helmet	26,296	Hexahedral C3D8R	4 mm
OA foams	105,628	Hexahedral C3D8R	4 mm
Mandible guard	20,738	Tetrahedral C3D10M	5 mm
Visor	19,844	Tetrahedral C3D10M	5 mm

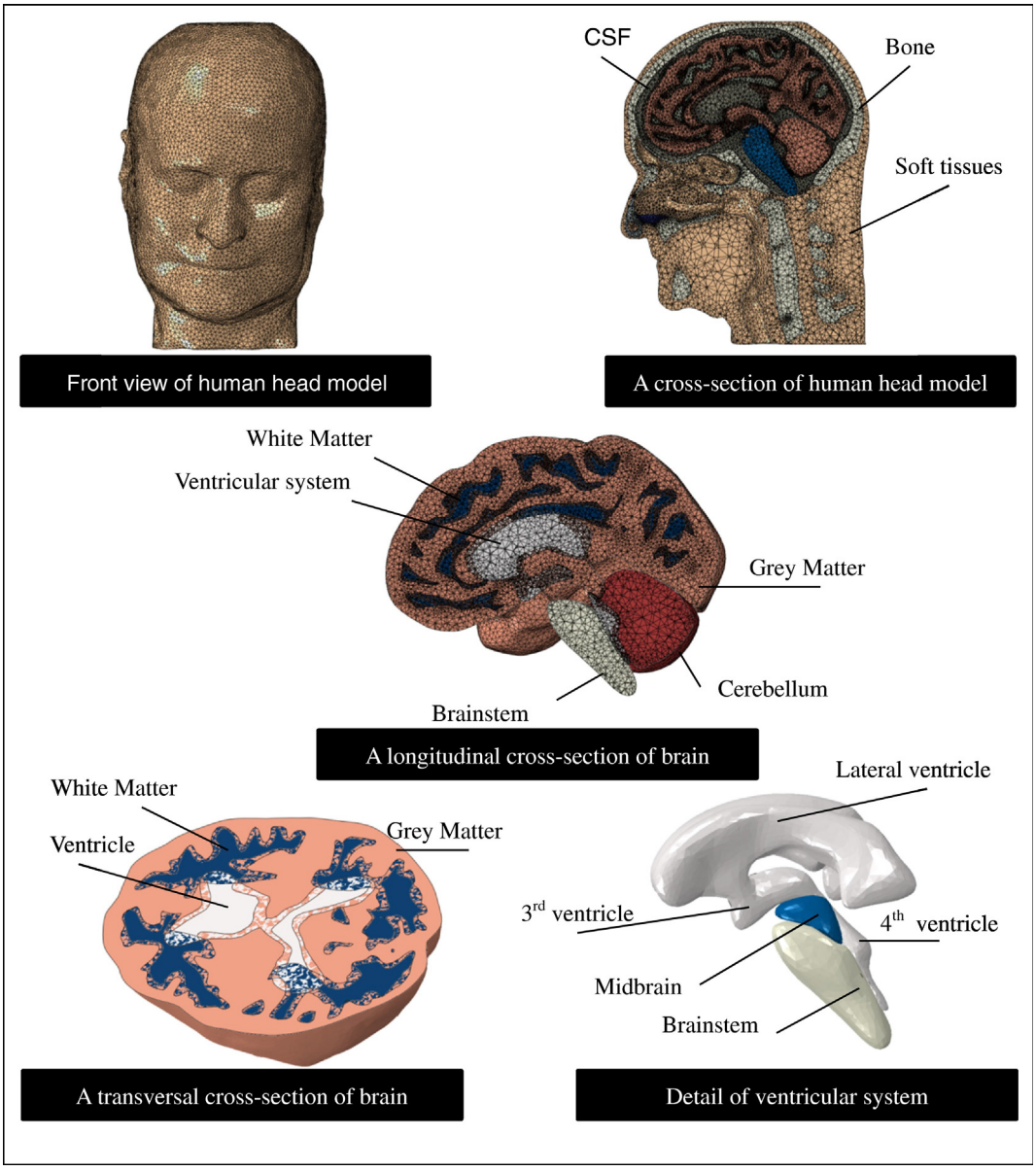

Fig. 3. Numerical model of human head and different details of its different components.

hyperelastic formulation whereby the strain energy potential is constructed numerically as a function of principal stretches and a set of internal variables associated with strain rate. The model is based on the assumption that the Poisson's ratio of the material is zero. With this assumption, the evaluation of the stress-strain response becomes uncoupled along the principal deformation directions. The model requires as input the stress-strain response of the material for both uniaxial tests. Rate-dependent behavior is specified by providing the uniaxial stress-strain curves for different values of nominal strain rates [47]. The mechanical behavior of the Oregon Aero (OA) foam padding is obtained from a previous paper [16,27], see Fig. 4a.

Table 2
Hashin damage criteria: failure modes for fiber and matrix.

Failure model	Hashin formulation
Tensile fiber failure ($\sigma_{11};\sigma_{22}>0$)	$d_{1t}=\left(\frac{\sigma_{11}}{X_{1T}}\right)^2+\left(\frac{\tau_{12}}{S_{12}}\right)^2+\left(\frac{\tau_{13}}{S_{13}}\right)^2$
	$d_{2t}=\left(\frac{\sigma_{22}}{X_{2T}}\right)^2+\left(\frac{\tau_{12}}{S_{12}}\right)^2+\left(\frac{\tau_{23}}{S_{23}}\right)^2$
Compressive fiber failure ($\sigma_{11};\sigma_{22}<0$)	$d_{1C}=\left(\frac{\sigma_{11}}{X_{1C}}\right)^2+\left(\frac{\tau_{12}}{S_{12}}\right)^2+\left(\frac{\tau_{13}}{S_{13}}\right)^2$
	$d_{2C}=\left(\frac{\sigma_{22}}{X_{2C}}\right)^2+\left(\frac{\tau_{12}}{S_{12}}\right)^2+\left(\frac{\tau_{23}}{S_{23}}\right)^2$
Tensile matrix failure ($\sigma_{33}>0$)	$d_{mt}=\left(\frac{\sigma_{33}}{X_{3T}}\right)^2+\left(\frac{\tau_{13}}{S_{13}}\right)^2+\left(\frac{\tau_{23}}{S_{23}}\right)^2$
Compressive matrix failure ($\sigma_{33}<0$)	$d_{mt}=\left(\frac{\sigma_{33}}{X_{3C}}\right)^2+\left(\frac{\tau_{13}}{S_{13}}\right)^2+\left(\frac{\tau_{23}}{S_{23}}\right)^2$

Table 3
Failure properties of Kevlar [15,27,46].

X_{1T} (MPa)	X_{1C} (MPa)	X_{2T} (MPa)	X_{2C} (MPa)	X_{3T} (MPa)	X_{3C} (MPa)	S_{12} (MPa)	S_{13} (MPa)	S_{23} (MPa)
555	555	555	555	1050	1050	77	1060	1086

- *Mandible guard*

The mandible guard is made of Kevlar composite and micro-agglomerated cork (MAC) since Coelho et al. [48] demonstrated that it is a good energy absorption system. The MAC is also modeled using the Low Density Foam material model, described previously. The stress-strain response of the MAC is obtained from Coelho et al. [48], (see Fig. 4b).

- *Visor*

The visor is made of polycarbonate. The mechanical behavior of polycarbonate was modeled using the Johnson-Cook model. Although this constitutive model is mainly applied to metals, it is also proper for polycarbonate as it is proposed by Dwivedi et al. [49]. The parameters of the JC equation were also obtained from this reference.

2.2.3. Head model

Mechanical modeling of the human head is complex due to the diversity of components being part of the head. Details of the modeling of the different parts of the head are provided below.

- *Bone and skeletal tissues.*

Although bone is an anisotropic material [50] due to the complex structure of the human skull, it is modeled as isotropic linear elastic material similar to other skeletal tissues such as cartilages and cervical vertebrae. This approach is accurate enough for the application achieved in this work.

- *Brain tissues.*

The brain tissues are modeled using a linear viscoelastic model combined with large deformation theory. The behavior of these tissues are characterized as viscoelastic behavior in shear with a deviatoric stress rate dependence on the shear relaxation modulus according to Ruan's work [51]. The viscoelastic shear behavior of the brain has been expressed by Eq. (1).

$$G(t) = G_\infty + (G_0 - G_\infty)e^{-\beta t} \tag{1}$$

where G_∞ is the long-term shear modulus measured in MPa; G_0 is the short-term shear modulus in MPa; and β is the decay factor in s^{-1}. All the material properties of the skull and brain tissues can be found in our previous work [36,37].

2.3. Boundary conditions

A restriction of the movement in all directions has been used at the base of the neck in order to fix the model. The ACH, together with the foam inserts, is mounted to the human head using gravity loading. This allows the interior foams to be deformed to fit the contours of the scalp of the head, as well as to provide a realistic helmet load onto the head surfaces without over stressing the head even before the blast impact step. The snug fitting and gravity load, together with nodes restraining the vertical displacement of the helmet, helps maintain the fitted configuration throughout the blast sequence. The interfaces between the helmet and interior cushions as well as between the cushions and head are modeled with the static-kinetic exponential decay frictional sliding contact.

For a real world scenario, both the blunt and blast impacts can cause rotational movement or removal of the helmet, thus it is necessary to fix it with auxiliary systems. However, this work simulates a particular case consisting of a frontal blast load that contributes very little to effects causing helmet removal or rotation. It is observed from the simulations that the relative movement between head and helmet is reduced to horizontal motion due to the frontal pressure loading. Moreover, previous works of the authors [15,37] have studied the effect of chin strap restraint in helmet performance showing a negligible effect under normal loading. Furthermore, to the authors' best knowledge, the chin strap restraint was not modeled in the literature [5,20,32,34].

Concerning contact inside the human head, a tangential sliding boundary condition with a friction coefficient equal to 0.2 is taken into account [28] on the interfaces between skull and CSF as well as between CSF and brain tissues. Moreover, tie constraints have been used in the interfaces between other intracranial contents and those between skull and cartilages.

2.4. Blast loading

In order to reproduce a shock wave, the CONWEP tool (CONventional WEaPon) implemented in the ABAQUS/Explicit [47] is used. CONWEP can be defined as a tool based on a pressure profile that characterizes the effect of conventional weapons for numerous events: air blast routines, breach, cratering, ground shock, and fragment and projectile penetrations etc. CONWEP assumes an exponential decay of the pressure with time developed by Friedlander [52], Eq. 2.

$$p(t) = p^*(1 - t/t^*)e^{-\beta t/t^*} \tag{2}$$

Where $p(t)$ is the overpressure at the time after detonation, $p^*$is the peak overpressure, t^* is the duration of the shock wave, and β is the decay constant. Fig. 5 shows the evolution of the overpressure with time after detonation. Panzer et al. [53] suggested the ranges of p^* and t^* between 50–1000 kPa and 1–8 ms respectively for obtaining the TBI. The Friedlander waveform is commonly used for the blast analysis [14,54]

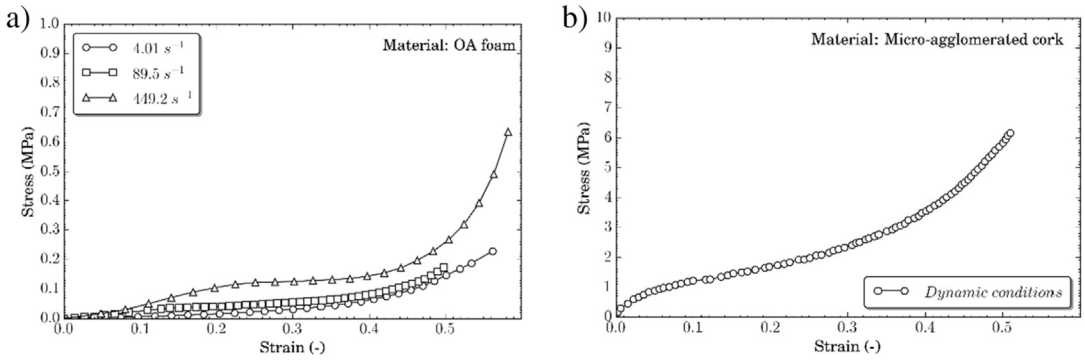

Fig. 4. The stress-strain response for: a) OA foams and; b) micro-agglomerated cork

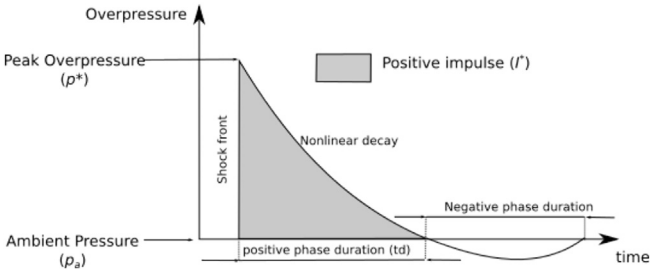

Fig. 5. Schematic of Friedlander wave.

In order to obtain the peak overpressure and the duration of the shock wave, Kinney and Graham [55] proposed respectively the Eqs. (3) and (4).

$$p^* = 808\,P_{atm}\cdot\frac{\left[1+\left(\frac{Z}{4.5}\right)^2\right]}{\sqrt{\left[1+\left(\frac{Z}{0.048}\right)^2\right]\left[1+\left(\frac{Z}{0.32}\right)^2\right]\left[1+\left(\frac{Z}{1.35}\right)^2\right]}} \tag{3}$$

$$\frac{t^*}{W^{\frac{1}{3}}} = \frac{980\cdot\left[1+\left(\frac{Z}{0.54}\right)^{10}\right]}{\sqrt{\left[1+\left(\frac{Z}{0.02}\right)^3\right]\left[1+\left(\frac{Z}{0.74}\right)^6\right]\left[1+\left(\frac{Z}{6.9}\right)^2\right]}} \tag{4}$$

Where p^* is the peak overpressure expressed in bars as well as the atmospheric pressure, P_{atm}; W is the mass of TNT in kg and Z the scaled distance and it is defined with a dimensionless parameter $Z = \frac{R}{W^{\frac{1}{3}}}$.

The levels of overpressure and associated pulse duration of a forward-facing blast were selected based on study developed by Fallah et al. [56]; this work considered a value of a stand-off distance, R, of 400 mm (representing a landmine detonation experienced by infantry soldiers). The net weight of TNT explosives determined was 100 g which lead to a peak pressure of 1.38 MPa and associated pulse duration of 0.17 ms for the forward-facing blast. Although it could be interesting the influence of pulse duration and peak pressure these variables are assumed to be constant for simplicity and high enough to be lethal according to Kinney's work [55]. The objective of the paper is comparing the performance of the different protection configurations and analyzing

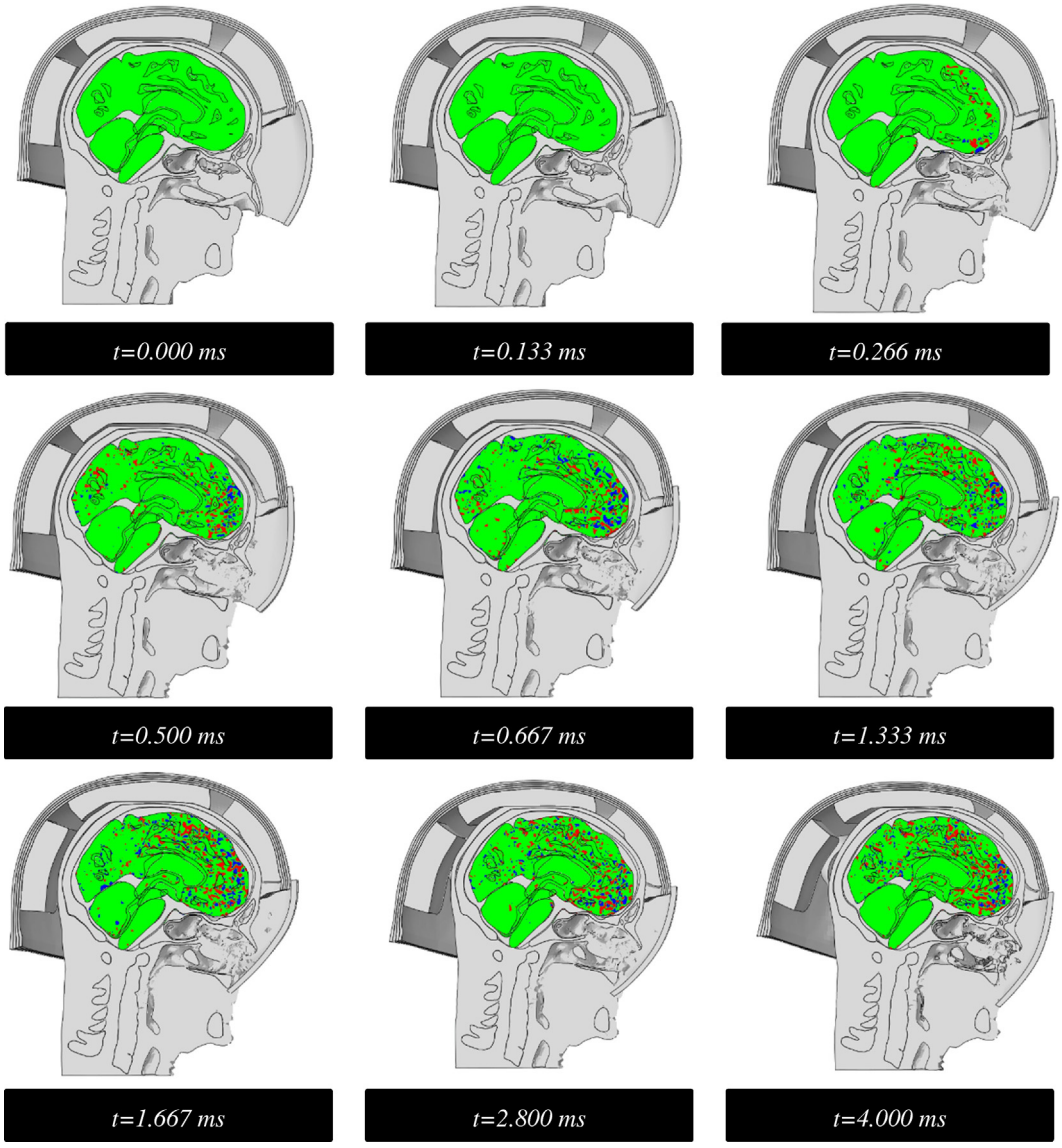

Fig. 6. Pressure contours of the brain. Case: helmet + visor. Red: greater than 235 and lower than −235 kPa; blue: between 173 kPa and 235 kPa or between −173 kPa and −235 kPa and yellow: between −173 kPa and 173 kPa. (For interpretation of the references to color in this figure legend, the reader is referred to the web version of this article.)

the ability of the different brain injuries criteria to predict damage for a given blast load.

3. Results and discussion

Simulations of a blast wave interacting with different configurations of the head and protections (head + helmet, head + helmet + visor, head + helmet + mandible guard and head + helmet + mandible guard + visor) were carried out using ABAQUS/Explicit. The analysis of the performance of these personal protections is described in terms of intracranial pressure (ICP), principal strain, shear strain and stress in the skull.

3.1. Brain injuries

The assessment of brain injury has been carried out using intracranial parameters such as intracranial pressure (ICP), principal and shear strain which are commonly used in the literature. In order to analyze the intracranial pressure injury, the ICP criterion, developed by Ward et al. [13] has been used. Thus, the peak intracranial pressure of >235 kPa would induce serious cerebral contusion, while minor or no brain injury would occur when the intracranial pressure was below 173 kPa. And, between 173 kPa and 235 kPa, minor contusion or cortex hemorrhage would occur.

- *Helmet + visor.*

The sagittal and axial views of the brain pressure contours for the helmet with visor is shown in Fig. 6. The peak positive pressures of >235 kPa is reached at the frontal lobe at $t = 0.133$ ms. Gradually, serious cerebral contusions appear from frontal lobe to occipital lobe and at $t = 0.266$ ms, the brain has been almost completely damaged.

- *Helmet + mandible guard.*

Fig. 7 shows the sagittal and axial views of the brain pressure contours for the helmet with mandible guard. Up to $t = 0.133$ ms, no serious cerebral contusions appear and this is localized in occipital lobe. With time progression the damage appears and extends in the brain, however, less density of damage is obtained when compared with the previous case.

- *Helmet + visor + mandible guard.*

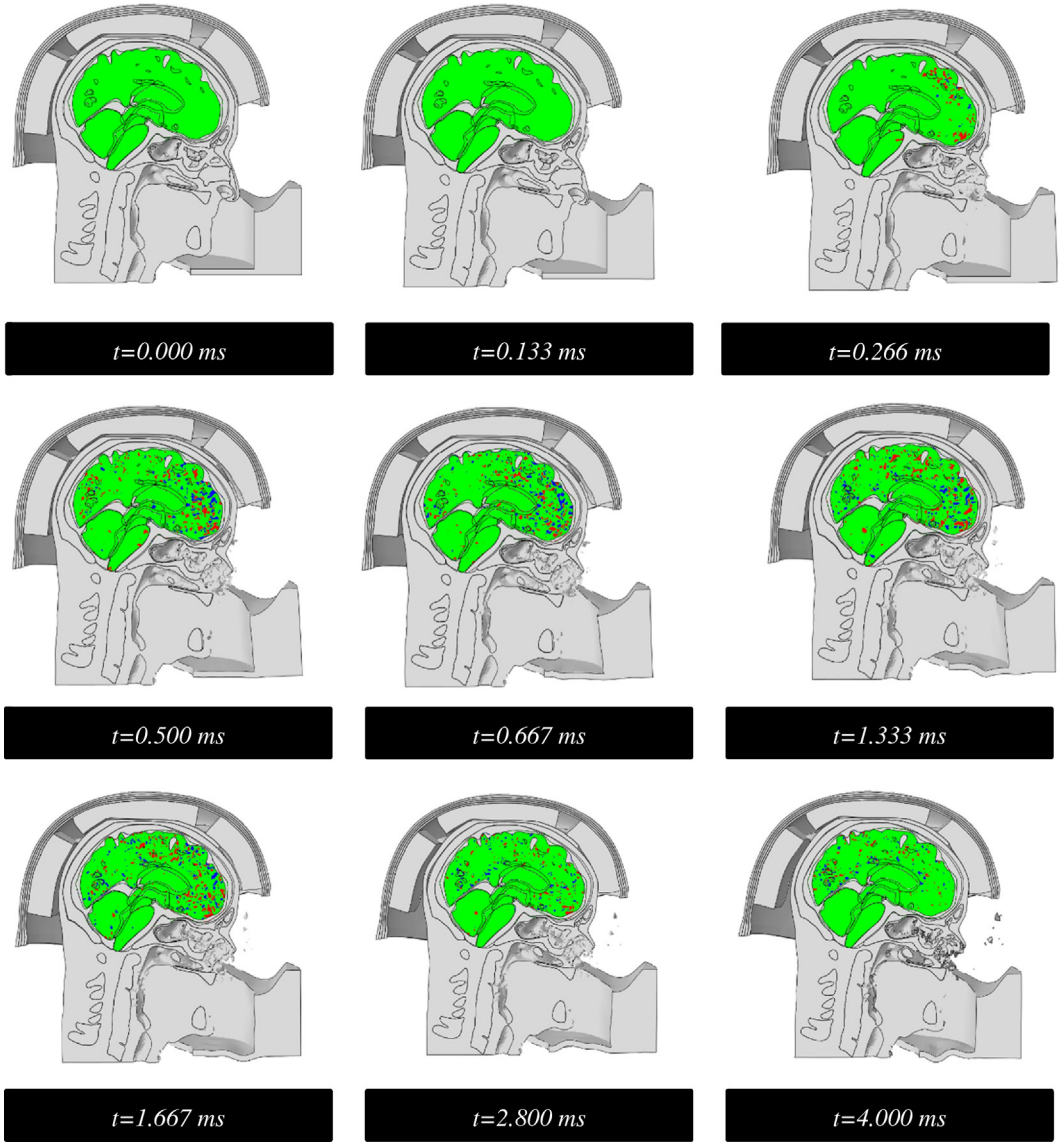

Fig. 7. Pressure contours of the brain. Case: helmet + mandible guard. Red: greater than 235 and lower than −235 kPa; blue: between 173 kPa and 235 kPa or between −173 kPa and −235 kPa and yellow: between −173 kPa and 173 kPa. (For interpretation of the references to color in this figure legend, the reader is referred to the web version of this article.)

The complete protection is modeled in this case; notable differences may be observed in Fig. 8 when compared with previous cases. The time corresponding to the appearance of peak positive pressures over 235 kPa is delayed until $t = 1.333$ ms, being the extension of the critical zones much more reduced than in the former cases. Similar behavior is observed at the time $t = 2.800$ ms, with a damaged area much more reduced than in the previous cases.

A comparison of the three cases is shown in Fig. 9 where intracranial pressure at the frontal, occipital and parietal lobe is plotted against time.

In the case of ICP in the frontal lobe, high ICP is observed at 1.75 ms for the helmet with visor protection and the helmet with mandible guard while that for the full model is at 3.3 ms. This behavior was also observed by other similar studies [15,34]. The use of mandible guard yielded greater mitigation of the ICP than the case of the use of visor because the peak pressure is around 2.04 MPa for the helmet + visor model while the peak pressure is around 1.77 MPa for the helmet + mandible guard model. In the case of ICP in the occipital lobe and parietal lobe, the use complete protection reduces until three times the damage effect. Table 4 shows the brain pressure contours at maximum values of ICP for the different cases. The maximum values of ICP are obtained for the case helmet + visor, while the minimum values are for complete full helmet. Note that the values calculated in this table are from the average of ten different points in the localization.

The use of principal strains and shear strains as a measure of brain injury has frequently been used in the literature [10–12]. Maximum principal strains had been demonstrated by Morrison et al. [57] as a predictor of central nervous system injuries such as diffuse axonal injury (DAI), cell death, and neuronal dysfunction when this parameter is higher than 0.2. While shear strains based on injury thresholds have been proposed by Zhang et al. [12] in the prediction of possibility of brain system injury when shear strains are higher than 0.14 with a 25% probability of moderate TBI.

Fig. 10 shows the history plots of the principal strain at the frontal, occipital and parietal lobe. In general, the full model is definitely the best option to reduce the amount of principal strain, except for the frontal lobe. The increase in the frontal lobe strains is caused by the severe deflection of the visor which subsequently hits the face. In all cases and configurations, principal strains obtained are significantly lower than the value proposed by Morrison et al. [57] as injury thresholds. The maximum principal strains are summarized in Table 5.

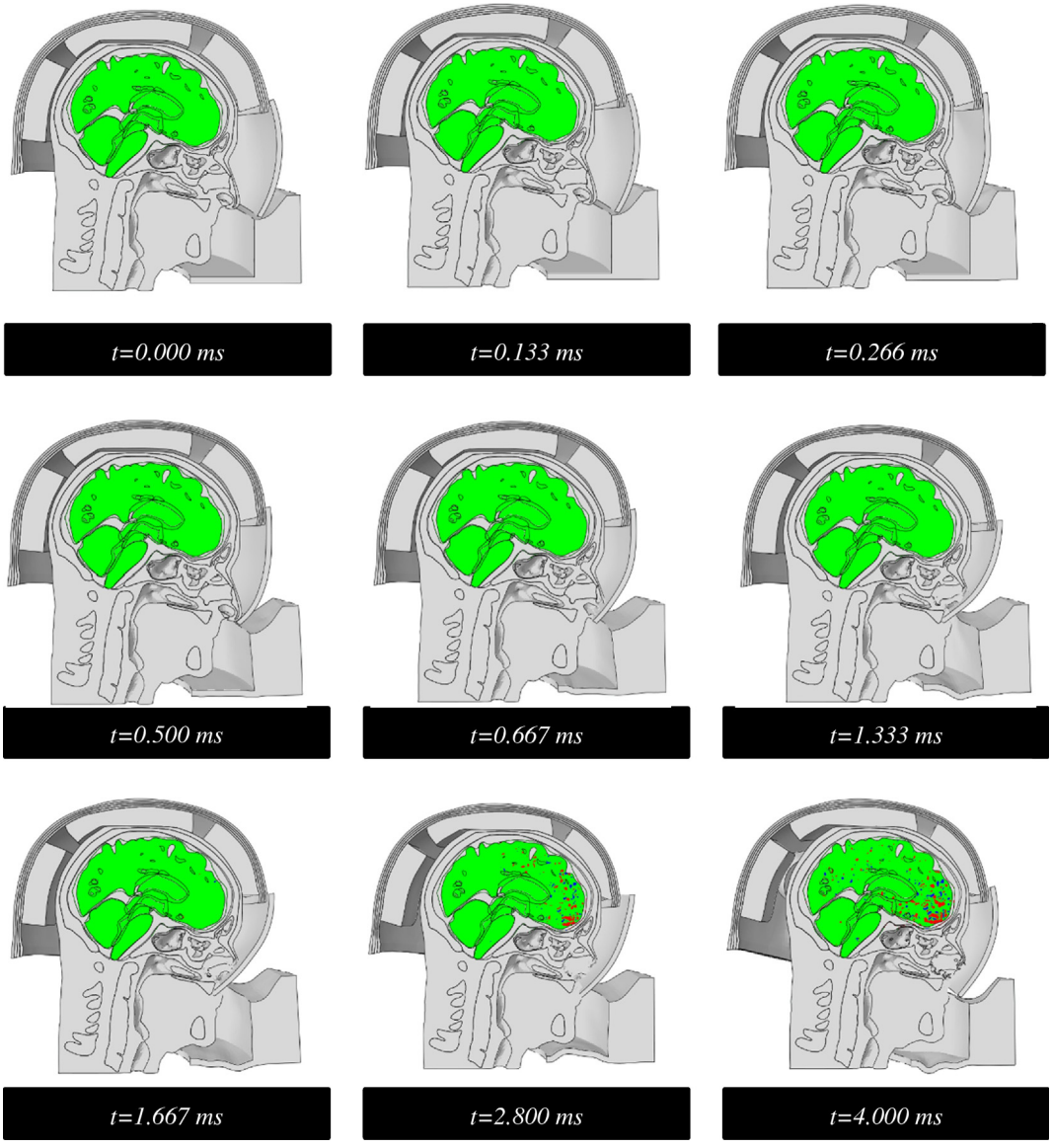

Fig. 8. Pressure contours of the brain. Case: helmet + visor + mandible guard. Red: greater than 235 and lower than −235 kPa; blue: between 173 kPa and 235 kPa or between −173 kPa and −235 kPa and yellow: between −173 kPa and 173 kPa. (For interpretation of the references to color in this figure legend, the reader is referred to the web version of this article.)

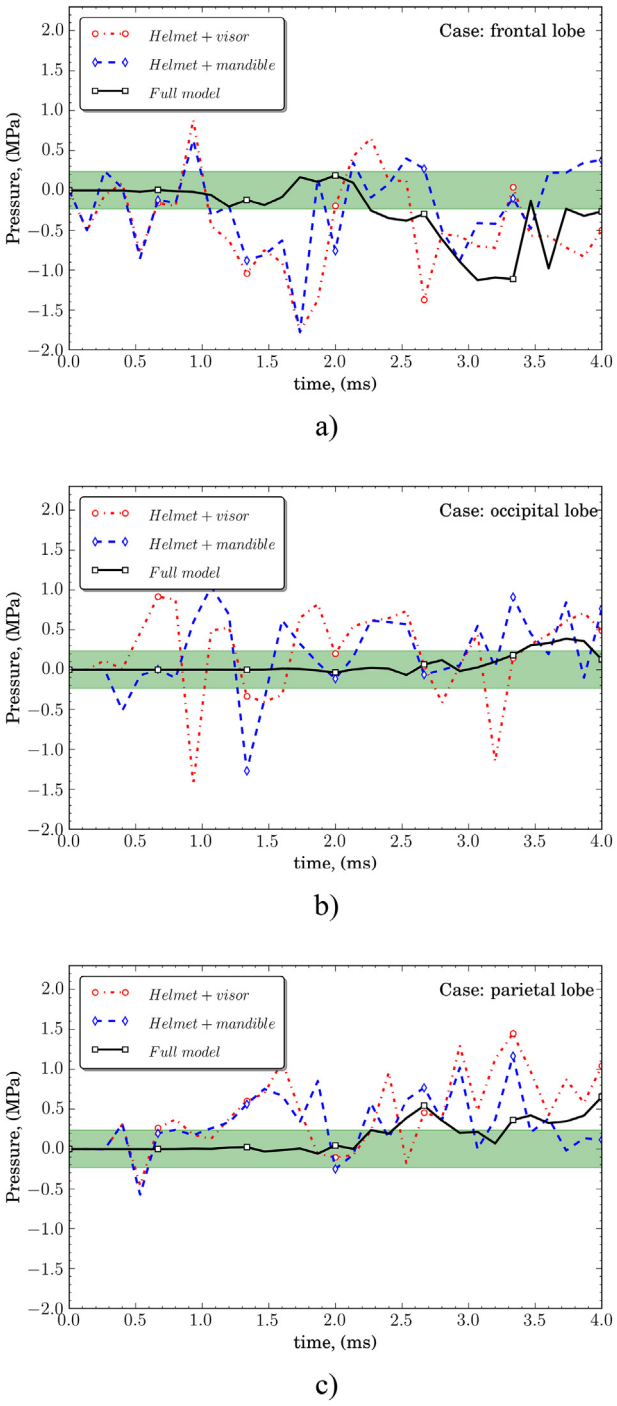

Fig. 9. Comparison of intracranial pressure (ICP) history of the brain tissues for the different configurations used and at different anatomical locations: a) frontal lobe; b) occipital lobe and; c) parietal lobe. The green region denotes no severe brain injuries. (For interpretation of the references to color in this figure legend, the reader is referred to the web version of this article.)

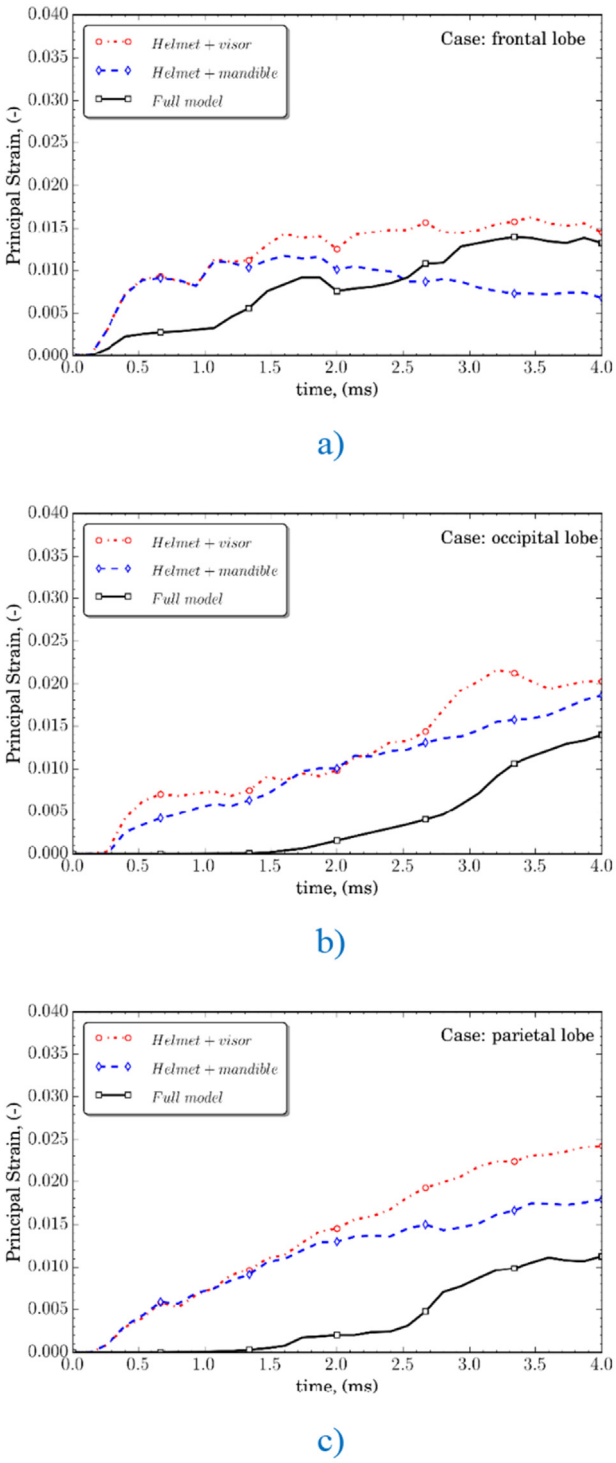

Fig. 10. Comparison of principal strain history of the brain tissues for the different configurations used and at different anatomical locations: a) frontal lobe; b) occipital lobe and; c) parietal lobe.

Table 4
Peak ICPs for different locations of blast.

	Frontal		Occipital		Parietal	
	Max	Min	Max	Min	Max	Min
Helmet + visor.	2.0442	−2.9447	2.0389	−1.9393	2.1556	−0.6192
Helmet + mandible guard.	1.7716	−2.9338	1.9223	−1.6074	1.8290	−0.7476
Helmet + visor + mandible guard.	0.3641	−1.2905	0.5122	−0.1237	0.7403	−0.1456

Table 5
Peak principal strains for different locations of blast.

	Frontal	Occipital	Parietal
Helmet + visor.	0.0165	0.0218	0.0245
Helmet + mandible guard.	0.0120	0.0186	0.0180
Helmet + visor + mandible guard.	0.0141	0.0140	0.0140

Similar trend is observed for shear strains, as shown in Fig. 11. The initial increase in shear strains occurs earlier in both the helmet + visor and helmet + mandible guard configurations than full helmet configuration,

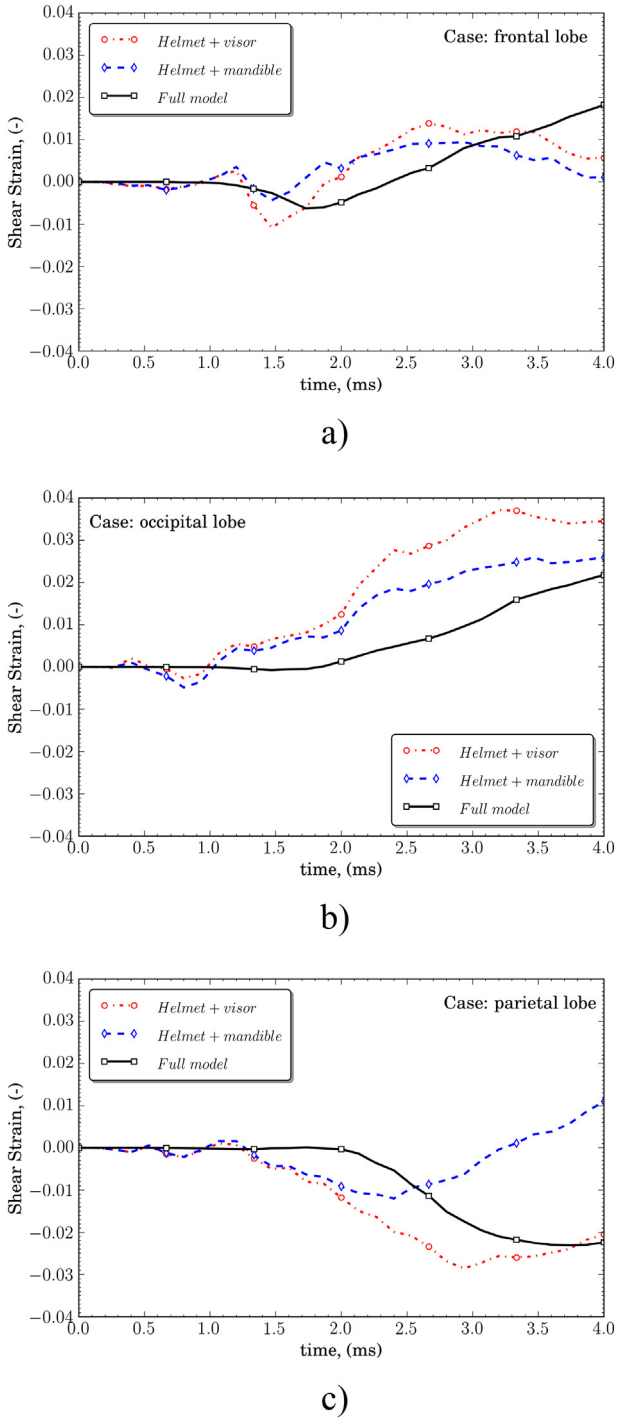

Fig. 11. Comparison of shear strain history of the brain tissues for the different configurations used and at different anatomical locations: a) frontal lobe; b) occipital lobe and; c) parietal lobe.

with higher magnitudes. However, beyond 3 ms of the blast impact, the frontal lobe shear strain in the full helmet configuration begins to pick up, while the frontal shear strains in the other two configurations declines gradually. This is mainly due to the "rear effect" of the visor, in which the visor deflects significantly under the extreme blast loading condition and the interior rear part of the visor hits the mid face region of the military personnel. It is highlighted that in all the configurations and anatomical landmarks, maximum shear strains are significantly lower than the limit value proposed by Zhang et al. [12]. The maximum shear strains are summarized in Table 6.

Therefore, the analysis of principal and shear strains revealed that no brain injury occurs according to limits mentioned earlier on [14,57]. The delay of peak value of all variables considered involved in the use of auxiliary protection is positive since it is related to damage decrease.

3.2. Structural response of the skull simulant

For the evaluation of the structural response of the skull, the von Mises stresses were examined at a frontal point of the skull. In this context the yield stress of 65 MPa of the skull bone was considered according to [13]. The results for the different cases analyzed are summarized below:

- *Helmet + visor.*

Fig. 12 shows the von Mises stress contours on the skull for the helmet with visor protection. High stresses are observed at the front of the skull that sequentially propagate to the parietal and rear of the skull. The maximum stresses during blast loading are located close to the nose part of the skull. This was due to visor protection impacting to head. At 2.00 ms, elevated stresses are observed at the neck in the basis of the skull.

- *Helmet + mandible guard.*

Different skull response is obtained when considering the helmet with mandible guard as shown in Fig. 13. Stresses are observed at the front of the skull, which sequentially propagate to the parietal and rear of the skull but, no concentration of stresses in the nose part appeared. The distribution is more uniform as observed at $t = 0.666$ ms.

- *Helmet + visor + mandible guard.*

In the case of full model, Fig. 14 shows that the propagation of stresses is barely noticeable However, under blast overpressures of larger magnitude and duration, tissue shearing at the eye brows and damage to the nose and neck may occur as reported by Taber et al. [7]. Due to use of visor, the impact of the visor onto the palate is observed at $t =$ 1.333 ms. Despite the impact occurrence, no skull damage is observed for this case.

A comparison of the evolution with time of the maximum Von Mises stress for the three configurations in the frontal of the skull is shown in Fig. 15. The results show that complete protection may reduce the magnitude of stress at the frontal area of the head. Full helmet protection resulted in the maximum value of stress of around 12 MPa and therefore fulfills the essential requirements of the stress thresholds in the cranial bone (65 MPa) according to Wood [19]. However, an incomplete or deficient protection could bring serious consequences in the cranial bone by going beyond the critical value of stress. The maximum Von Misses stress is found in the cranial bone for the use of helmet + visor or helmet + mandible guard. For the full model, this maximum value is obtained in the palate where the consequences are less severe.

4. Conclusions

In this paper, numerical analysis of the complete helmet design including protective equipment was analyzed. The mitigation effect of protective equipment on the head response due to blast impact was

Table 6
Peak shear strains for different locations of blast.

	Frontal		Occipital		Parietal	
	Max	Min	Max	Min	Max	Min
Helmet + visor.	0.0148	−0.0109	0.0373	−0.0033	0.0019	−0.0288
Helmet + mandible guard.	0.0097	−0.0044	0.0260	−0.0054	0.0110	−0.0121
Helmet + visor + mandible guard.	0.0182	−0.0064	0.0218	−0.0008	0.0003	−0.0233

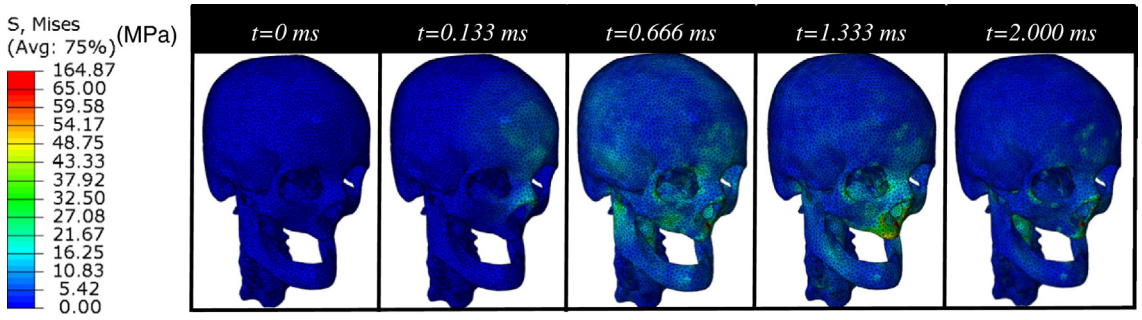

Fig. 12. Mises stress contours of the skull. Case: helmet + visor.

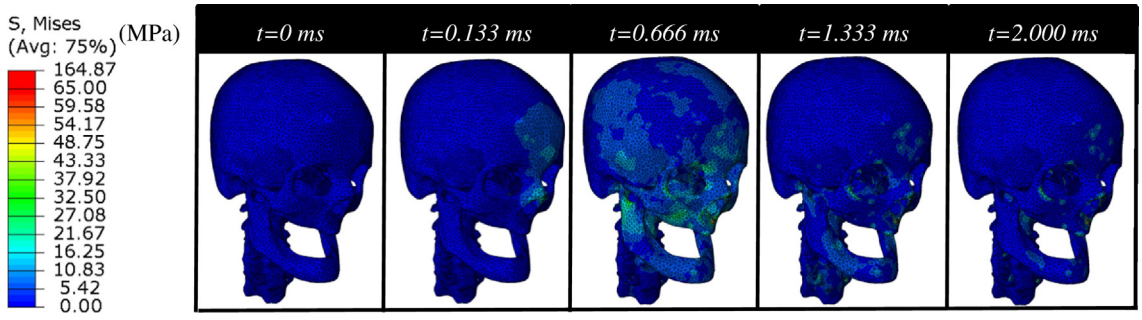

Fig. 13. Mises stress contours of the skull. Case: helmet + mandible guard.

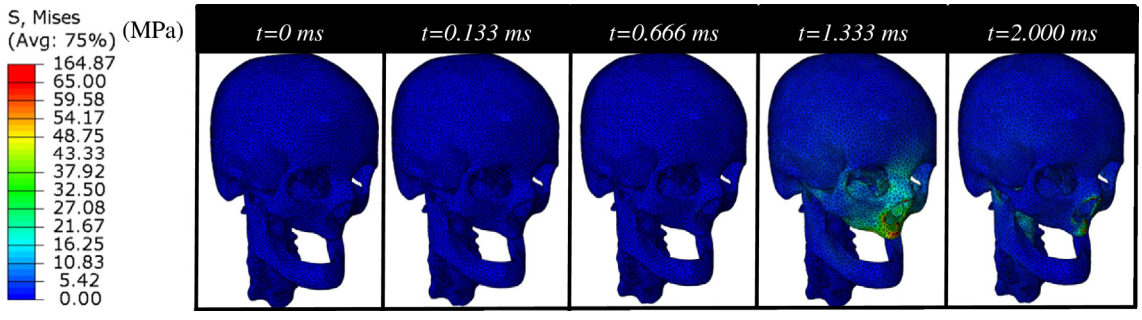

Fig. 14. Mises stress contours of the skull. Case: helmet + visor + mandible guard.

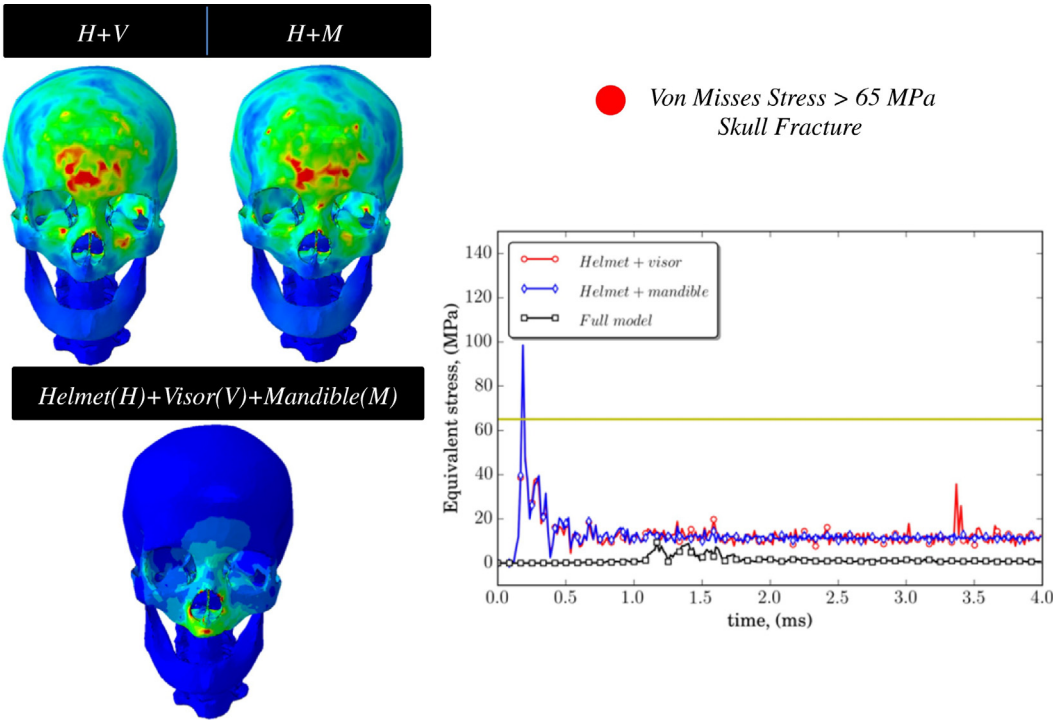

Fig. 15. Comparison of maximum Von Misses stress of skull for the different cases.

presented using ABAQUS. The single frontal blast simulation is conducted by applying the Friedlander blast profile using the CONWEP tool implemented in ABAQUS.

Based on the ICP threshold for brain injuries and stress threshold for skull fractures, it was demonstrated that serious injuries may occur for the helmet with individual protective equipment. However, the presence of protective equipment reduces the brain pressures by 5 times and ensures that no fracture in the skull appears. Nevertheless, based on the thresholds for principal and shear strains, no brain injuries occur. It is worth noting that the ICP criterion is the most restrictive indicating brain injuries while principal and shear strains criteria show values under threshold damage. The use of protective equipment delays occurrence of maximum peak of all damage variables considered (pressure, principal and shear strains). The influence of pulse duration in final resultant brain damage illustrates the advantages of using these auxiliary systems. It is important to make considerable efforts in the designing of adequate helmet protection to ensure soldier's protection during the unfortunate event of multiple consecutive blasts. The successful implementation of the visor and mandible guard to achieve specific mitigation targets requires their optimization considering both loading and ergonomic aspects. The contributions presented in this work could help during the design of personal protection.

Acknowledgement

The authors acknowledge the Ministry of Economy and Competitiveness of Spain and FEDER program under the Project RTC-2015-3887-8 for the financial support of the work.

References

[1] M.D. Sue Binder, Report to Congress on Mild Traumatic Brain Injury in the United States: Steps to Prevent a Serious Public Health Problem, Centers for Disease Control and Prevention, Atlanta (GA), 2003.
[2] DMSS, Defense Medical Surveillance System (DMSS), Theater Medical Data Store (TMDS) Provided by the Armed Forces Health Surveillance Center (AFHSC). Prepared by the Defense and Veterans Brain Injury Center (DVBIC)Available at: http://dvbic.dcoe.mil/sites/default/files/uploads/2000-2013_dod-tbi-worldwide-2000-2013-13_02-26-14.pdf2013 (accessed 28.8 2016).
[3] C. Wang, J.B. Pahk, C.D. Balaban, M.C. Miller, A.R. Wood, J.S. Vipperman, Computational study of human head response to primary blast waves of five levels from three directions, PLoS One 9 (2014), e113264. .
[4] S.G. Kulkarni, X.L. Gao, S.E. Horner, J.Q. Zheng, N.V. David, Ballistic helmets — their design, materials, and performance against traumatic brain injury, Compos. Struct. 101 (2013) 313–331.
[5] S. Ganpule, A. Alai, E. Plougonven, N. Chandra, Mechanics of blast loading on the head models in the study of traumatic brain injury using experimental and computational approaches, Biomech. Model Mech. 12 (2013) 511–531.
[6] G.A. Elder, E.M. Mitsis, S.T. Ahlers, A. Cristian, Blast-induced mild traumatic brain injury, Psychiatr. Clin. N. Am. 33 (2010) 757–781.
[7] K.H. Taber, D.L. Warden, R.A. Hurley, Blast-related traumatic brain injury: what is known? J. Neuropsych. Clin. N. 18 (2006) 141–145.
[8] J.H. Stuhmiller, Blast injury: translating research into operational medicine. In quantitative physiology: problems and concepts in military operational medicine, in: W. Santee, K. Friedl (Eds.), Textbook of Military Medicine, Office of the Surgeon General at TMM Publications, Borden Institute, Walter Reed Army Medical Centre, U.S. Army Medical Department Centre and School, 2008.
[9] H.R. Champion, J.B. Holcomb, L.A. Young, Injuries from explosions: physics, biophysics, pathology, and required research focus, J. Trauma 66 (2009) 1468–1477.[10] K.M. Tse, L.B. Tan, B. Yang, V.B.C. Tan, H.P. Lee, Effect of helmet liner systems and impact directions on severity of the head injuries sustained in ballistic impacts: a finite element (FE) study, Med. Biol. Eng. Comput. (2016) 1–22.
[11] K.M. Tse, S.P. Lim, V.B.C. Tan, H.P. Lee, A review of head injury and finite element head models, Am. J. Eng. Technol. Soc. 1 (5) (2014) 28–52.
[12] L. Zhang, K.H. Yang, A.I. King, A proposed injury threshold for mild traumatic brain injury, J. Biomech. Eng. 126 (2004) 226–236.
[13] C. Ward, M. Chan, A. Nahum, Intracranial pressure — a brain injury criterion, Proc. 24th Stapp Car Crash Conf. (1980) 163–185.
[14] S. Kleiven, Biomechanics and thresholds for MTBI in humans, MTBI Pre-Congress Symp., Lisbon, Portugal, 2008.
[15] L.B. Tan, K.M. Tse, H.P. Lee, V.B.C. Tan, S.P. Lim, Performance of an advanced combat helmet with different interior cushioning systems in ballistic impact: experiments and finite element simulations, Int. J. Impact Eng. 50 (2012) 99–112.
[16] L.B. Tan, F.S. Chew, K.M. Tse, V.B.C. Tan, H.P. Lee, Impact of complex blast wave on the human head: a computational study, Int. J. Num. Method Biomed. Eng. (2014) 1–30.
[17] D. Singh, D.S. Cronin, T.N. Haladuick, Head and brain response to blast using sagittal and transverse finite element models, Int. J. Num. Method Biomed. Eng. 30 (2014) 470–489.
[18] J.H. McElhaney, J.L. Fogle, J.W. Melvin, R.R. Haynes, V.L. Roberts, N.M. Alem, Mechanical properties of cranial bone, J. Biomech. 3 (1970) 495–511.
[19] J.W. Wood, Dynamic response of human cranial bone, J. Biomech. 4 (1970) 1–12.
[20] M.K. Nyein, A.M. Jason, L. Yu, C.M. Pita, J.D. Joannopoulos, D.F. Moore, R.A. Radovitzky, In silico investigation of intracranial blast mitigation with relevance to military traumatic brain injury, P. Natl. Acad. Sci. USA 107 (2010) 20703-1–20703-8.
[21] A. Saljo, M. Mayorga, H. Bolouri, B. Svensson, A. Hamberger, Mechanisms and pathophysiology of the low-level blast brain injury in animal models, NeuroImage 54 (2011) 83–88.

Fig. 15. Comparison of maximum Von Misses stress of skull for the different cases.

[22] M. Risling, J. Davidsson, Experimental animal models for studies on the mechanisms of blast-induced neurotrauma, Front. Neurol. (2012) 1–9.
[23] F. Zhu, C. Wagner, A.D.C. Leonardi, X. Jin, P. VandeVord, C. Chou, K.H. Yang, A.I. King, Using a gel/plastic surrogate to study the mechanical response of the head under air shock loading: a combined experimental and numerical investigation, Biomech. Model Mech. 11 (2011) 341–353.
[24] C.E. Needham, D. Ritzel, G.T. Rule, S. Wiri, L. Young, Blast testing issues and TBI: experimental models that lead to wrong conclusions, Front. Neurol. 6 (2015) 2–11.
[25] V. Tinard, C. Deck, R. Willinger, New methodology for improvement of helmet performances during impacts with regards to biomechanical criteria, Mater. Des. 37 (2012) 79–88.
[26] F.A. Pintar, M.M.G.M. Philippens, J. Zhang, N. Yoganandan, Methodology to determine skull bone and brain responses from ballistic helmet-to-head contact loading using experiments and finite element analysis, Med. Eng. Phys. 35 (2013) 1682–1687.

[27] M. Rodríguez-Millán, T. Ito, J.A. Loya, A. Olmedo, M.H. Miguélez, Development of numerical model for ballistic resistance evaluation of combat helmet and experimental validation, Mater. Des. 110 (2016) 391–403.
[28] P.A. Taylor, C.C. Ford, Simulation of blast-induced early-time intracranial wave physics leading to traumatic brain injury, J. Biomech. Eng. 131 (2009) 061007.
[29] P.A. Taylor, J.S. Ludwigsen, C.C. Ford, Investigation of blast-induced traumat i c b r a i n injury, Brain Inj. [BI] 28 (2014) 879–895.
[30] D.F. Moore, A. Jerusalem, M. Nyein, L. Noels, M.S. Jaffee, R.A. Radovitzky, Computational biology — modeling of primary blast effects on the central nervous system, NeuroImage 47 (2009) 10–20.
[31] M. Grujicic, G. Arakere, T. He, Material-modeling and structural-mechanics aspects of the traumatic brain injury problem, Multidiscip. Model. Mater. Struct. 6 (2009) 335–363.
[32] L. Zhang, R. Makwana, S. Sharma, Brain response to primary blast wave using validated finite element models of human head and advanced combat helmet, Front. Neurol. (2013) 1–12.
[33] H.P. Lee, S.W. Gong, Finite element analysis for the evaluation of protective functions of helmets against ballistic impact, Comp. Method Biomech. 13 (2010) 537–550.
[34] D. Jenson, V.U. Unnikrishnan, Energy dissipation of nanocomposite based helmets for blast-induced traumatic brain injury mitigation, Compos. Struct. 121 (2015) 211–216.
[35] Mott, T.R. Young, D.A. Schwer, Blast loading on the head under a military helmet: effect of face shield and mandible protection, 52nd Aerospace Sciences Meeting, 11, 2014, pp. 9142–9162.
[36] K.M. Tse, L.B. Tan, S.J. Lee, S.P. Lim, H.P. Lee, Development and validation of two subject-specific finite element models of human head against three cadaveric experiments, Int. J. Num. Methods Biomed. Eng. 30 (2014) 397–415.
[37] K.M. Tse, L.B. Tan, B. Yang, V.B.C. Tan, H.P. Lee, Effect of helmet liner systems and impact directions on severity of head injuries sustained in ballistic impacts: a finite el-ement (FE) study, Med. Biol. Eng. Comput. (2016) 1–22.
[38] R. Willinger, H.S. Kang, B. Diaw, Three-dimensional human head finite-element model validation against two experimental impacts, Ann. Biomed. Eng. 27 (1999) 403–410.
[39] T.J. Horgan, M.D. Gilchrist, Influence of FE model variability in predicting brain motion and intracranial pressure changes in head impact simulations, Int. J. Crashworthines 9 (2004) 401–408.
[40] A.M. Nahum, R. Smith, C.C. Ward, Intracranial pressure dynamics during head impact, 21st Stapp Car Crash Conference 1977, pp. 339–366 Society of Automotive En-gineers (SAE), SAE Paper No. 770922: San Diego, USA.
[41] X. Trosseille, C. Tarriere, F. Lavaste, Development of a FEM of the human head according to a specific test protocol, 30th Stapp Car Crash Conference 1992, pp. 235–253 Society of Automotive Engineers (SAE), SAE Paper No. 922527: Warrendale, USA.
[42] V.N. Hardy, C. Foster, M. Mason, K. Yang, A. King, S. Tashman, Investigation of head injury mechanisms using neutral density technology and high-speed biplanar X-ray, 45th Stapp Car Crash Conference, San Antonio, USA 2001, pp. 337–368.
[43] Z. Hashin, Failure criteria for unidirectional fiber composites, Trans. ASME J. Appl. Mech. 47 (1980) 329–334.
[44] M. Rodríguez-Millán, C.E. Moreno, M. Marco, C. Santiuste, H. Miguélez, Numerical analysis of the ballistic behaviour of Kevlar® composite under impact of doublenosed stepped cylindrical projectiles, J. Reinf. Plast. Comp. 35 (2016) 124–137.
[45] K.P. Pinnoji, P. Mahajan, Analysis of impact-induced damage and delamination in
[46] S.W. Gong, H.P. Lee, C. Lu, Computational simulation of the human head response to non-contact impact, Comput. Struct. 86 (2008) 758–770.
[47] Dassault Systèmes, Abaqus v6.12 Documentation-ABAQUS Analysis User's Manual. ABAQUS Inc; 6.12, 2012.
[48] R.M. Coelho, R.J. Alves de Sousa, F.A.O. Fernandes, F. Teixeira-Dias, New composite liners for energy absorption purposes, Mater. Des. 43 (2013) 384–392.
[49] A. Dwivedi, J. Bradley, D. Casem, Mechanical Response of Polycarbonate With Strength Model FitsArmy Research Laboratory 2012.
[50] C. Santiuste, M. Rodríguez-Millán, E. Giner, H. Miguélez, The influence of anisotropy in numerical modeling of orthogonal cutting of cortical bone, Compos. Struct. 116 (2014) 423–431.
[51] J.S. Ruan, Impact Biomechanics of Head Injury by Mathematical Modeling, Wayne State University, Detroit, 1994.
[52] F.G. Friedlander, The Wave Equation on a Curved Space-Time, Cambridge University Press, London, 1976.
[53] M.B. Panzer, B.S. Myers, B.P. Capehart, C.R. Bass, Development of a finite element model for blast brain injury and the effects of CSF cavitation, Ann. Biomed. Eng. 40 (2012) 1530–1544.
[54] M. Grujicic, W.C. Bell, B. Pandurangan, T. He, Blast-wave impact-mitigation capability of polyurea when used as helmet suspension-pad material, Mater. Des. 31 (2010) 4050–4065.

[55] G.F. Kinney, K.J. Graham, Explosive Shocks in Air, second ed. Springer-Verlag, New York, 1985.
[56] A.S. Fallah, K. Micallef, G.S. Langdon, W.C. Lee, P.T. Curtis, L.A. Louca, Dynamic response of Dyneema® HB26 plates to localised blast loading, Int. J. Impact Eng. 73 (2014) 91–100.
[57] B. Morrison 3rd, H.L. Cater, C.C. Wang, F.C. Thomas, C.T. Hung, G.A. Ateshian, L.E. Sundstrom, A tissue level tolerance criterion for living brain developed with an in vitro model of traumatic mechanical loading, Stapp. Car Crash J. 47 (2003) 93–105.